INSTITUTE OF PHYSICS PUBLISHING MEASUREMENT SCIENCE AND TECHNOLOGY

Meas. Sci. Technol. **16** (2005) 1667–1676 doi:10.1088/0957-0233/16/8/019

NICE: an instrument for direct mass spectrometric measurement of interstellar neutral gas

M Wieser[1], P Wurz[1], P Bochsler[1], E Moebius[2], J Quinn[2], S A Fuselier[3], A Ghielmetti[3], J N DeFazio[4], T M Stephen[4] and R J Nemanich[5]

[1] Physikalisches Institut, University of Bern, Sidlerstrasse 5, 3012 Bern, Switzerland
[2] Department of Physics and Inst. for Study of Earth, Oceans and Space, University of New Hampshire, Durham, NH 03824, USA
[3] Lockheed Research Laboratories, 3251 Hannover St, Palo Alto, CA 94304, USA
[4] Department of Physics and Astronomy, University of Denver, Denver, CO 80208, USA
[5] Department of Physics, North Carolina State University, 408A Cox, Box 8202, Raleigh, NC 27695, USA

E-mail: wieser@phim.unibe.ch

Received 24 February 2005, in final form 22 May 2005
Published 20 July 2005
Online at stacks.iop.org/MST/16/1667

Abstract
The direct measurement of the neutral interstellar gas requires a very sensitive neutral particle imaging instrument in the energy range of 10 eV–1000 eV. For successful detection and identification, the neutral particles have to be ionized first, which will be accomplished via surface ionization. This method is successfully employed in the Low Energy Neutral Atom imager (LENA) instrument on the IMAGE spacecraft launched on 25 March 2000, which still operates well. We present the laboratory prototype of the Neutral Interstellar Composition Experiment (NICE), a neutral particle mass spectrometer dedicated to the measurement of interstellar gas, and will discuss its instrumental characteristics. Performance is evaluated with emphasis on the neutral to negative ion conversion for hydrogen and oxygen and the collection of these ions by the mass spectrometer. Measurements of the detection efficiency of the prototype for primary neutral hydrogen and oxygen atoms are presented. Several conversion surfaces, conductive and insulating, were investigated and all are potential candidates for a next generation neutral particle imaging instrument.

Keywords: interstellar medium, energetic neutral atoms, surface ionization, mass spectrometry, imaging neutral atom detector

1. Introduction

Measurements of the physical parameters (temperature, density, composition and others) of the local interstellar medium (LISM) will give information about the evolution of the solar system and our galaxy. The LISM is separated from the solar system by the heliopause and charged interstellar particles cannot cross this boundary to enter the solar system. The neutral fraction of the LISM, however, is not subject to magnetic interactions and can therefore penetrate deeply into the solar system. As the Sun moves with a velocity of approximatively 26 km s^{-1} relative to the LISM a directed inflow of interstellar neutral atoms can be observed [1–4]. Furthermore, energetic neutrals are produced by charge exchange processes at the heliospheric boundary [5]. When approaching the Sun the neutral particle populations are affected by gravitation, photo ionization and charge exchange processes. For a spacecraft travelling from Earth towards the heliopause, at a distance of about a few astronomical units from

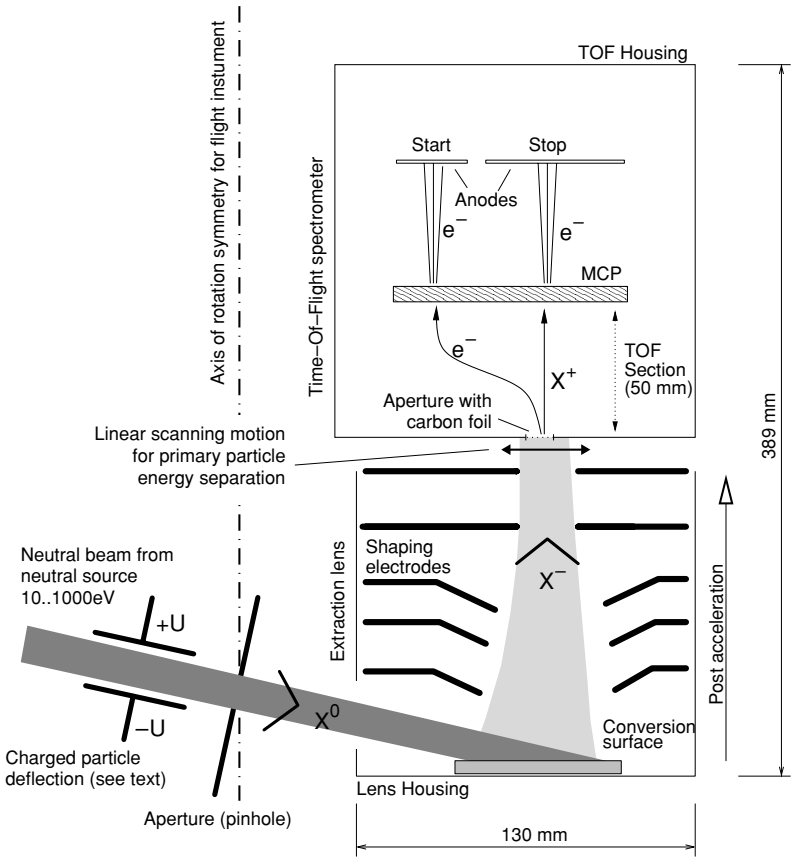

Figure 1. Schematic view of the NICE prototype with envelope dimensions. The indicated height includes the electronics box, power supplies and digital processing unit needed for the time-of-flight spectrometer.

the Sun these effects become negligible. Consequently, it is possible to infer the properties of the neutral interstellar gas by measuring the properties of the inflowing neutrals. This has been done for interstellar helium by the Neutral Interstellar Gas Instrument (GAS) on the Ulysses spacecraft [6]. The Ulysses mission was launched on 6 October 1990 and was brought into a polar orbit around the Sun on 2 August 1992 using a gravitational assist at Jupiter. Ulysses still operates and is in its third orbit around the Sun. The GAS instrument takes data at selected observation times when the LISM flow vector and the spacecraft position are favourable. Elements other than helium can potentially be measured directly using the surface ionization technique [7, 8]. Surface ionization is currently successfully employed by the Low Energy Neutral Atom imager (LENA) instrument on the IMAGE spacecraft for investigations of the terrestrial magnetosphere [9]. LENA surface conversion technology development started late 1992 at the University of Bern. The LENA instrument development started in fall 1995, after NASA's selection of IMAGE as a MIDEX mission.

We have built and tested the laboratory prototype of the Neutral Interstellar Composition Experiment (NICE) instrument for the detection of neutral hydrogen, carbon and oxygen atoms using the surface ionization technique. A velocity range of 10 km s^{-1} to 100 km s^{-1} corresponding to an energy range of 10 eV–1000 eV depending on species was investigated. This velocity range is expected for the inflow as seen from a spacecraft in a solar orbit or on an escape trajectory from the solar system. NICE is a pinhole camera with angular resolution along one dimension, allowing angularly resolved direct measurements of the interstellar gas flow on possible future missions, such as NASA mission concepts Interstellar Pathfinder [10], Interstellar Boundary Explorer [11], Realistic Interstellar Explorer [12] or Interstellar Probe [13].

2. Prototype instrument

Figure 1 shows a schematic drawing of the NICE prototype. Neutral particles enter the instrument through an aperture preceded by a charged particle deflection system that hinders charged particles from entering the system. For successful detection the incident neutrals must be ionized first, which is accomplished by surface ionization [14]. Upon reflection at grazing incidence from a suitable surface a fraction of the incident neutrals is negatively ionized (1%–30%) [15–17]. An electrostatic extraction lens collects and accelerates these ions before they are analysed in a time-of-flight mass spectrometer (TOF) and provides coarse primary particle energy resolution [7, 8]. Several different conversion surface materials were tested with the NICE prototype: a hydrogen passivated CVD diamond surface [17, 18], a polished MgO single crystal [16], a layered sample with a $BaZrO_3$ top layer [15, 19], and a polished poly-crystalline tungsten surface, the LENA/IMAGE flight spare surface [9]. The investigated conversion surfaces (CS) were all polished to a roughness of a few nm RMS, which

is necessary for good particle reflection with minimal angular scattering.

Negative ions originating from the entire conversion surface area are focused on a spot at the TOF entrance plane for all emission angles. The position of the spot is a function of the reflected particle energy. Angular scattering at the CS tends to broaden the focal spot. Because this effect is smaller than the energy dispersion of the lens, it is possible to extract moderate energy information from the position across the exit of the lens. Figure 3 depicts a SIMION [20] simulation of the focusing properties of the extraction lens, where a situation with the conversion surface CS on ground potential is shown. Neutral particles enter the lens from the left and are negatively ionized at the CS. Negative ions with three different energies after reflection (14 eV, 50 eV and 200 eV) and two different scattering angles from the surface (65°, dark colours, and 82°, light colours, to the surface normal) are shown. Particles with different energies are mapped to different positions at the image plane where the TOF entry aperture is located. Different scattering angles at the CS have only a minor influence on the position at the image plane (see inset in figure 3). In this simulation, the energy-resolved spectrum at the image plane is about 15 mm wide (depending on the energy range used) for a distance of 115 mm from the CS to the image plane.

The angle of the incident neutrals in a direction out of the paper plane in figure 1, the azimuth angle, is transformed into an angular position along the circular entry slit of the TOF section where the negative ions pass a carbon foil. After passing the carbon foil the particle has changed its charge state to positive and is detected at the stop micro-channel plate (MCP). Secondary electrons generated at the carbon foil are also deflected towards the MCP where they generate the start signal. Start and Stop signals are then used to obtain the time of flight. If the TOF unit can measure not only the time of flight of an ion, but also the position at its entrance in two dimensions, then three quantities of the detected particle are measured: mass, energy and azimuth angle [7, 8]. To minimize the effects of non-specular reflection on azimuth resolution (out of the paper plane in figure 1) it is necessary to apply a high extraction field near the CS and to have a high ratio of final to initial energy. A lens extraction voltage of 14 kV was used for the current tests compared to a energy below 1 keV per atom of the converted ions. A high ratio of final to initial energy also allows one to directly infer the particle mass from the time of flight. The spread in time of flight due to different incident neutral particle energies, the energy loss at the conversion surface and at the carbon foil are small enough to make a good separation of hydrogen, carbon and oxygen.

The TOF mass spectrometer used in our prototype was an adapted flight spare unit of the composition and distribution function analyser (CODIF) as being flown on the Cluster satellites [21], which is larger than necessary for the use in NICE since it covers 360° in azimuthal direction where only 180° is needed for NICE. In addition to the TOF unit, electronics and power supply sections of CODIF were utilized while the original CODIF entrance section was replaced by the NICE extraction lens as shown in figure 1. As the tests were performed with a collimated neutral beam, we did not make use of the angular position sensing capability of

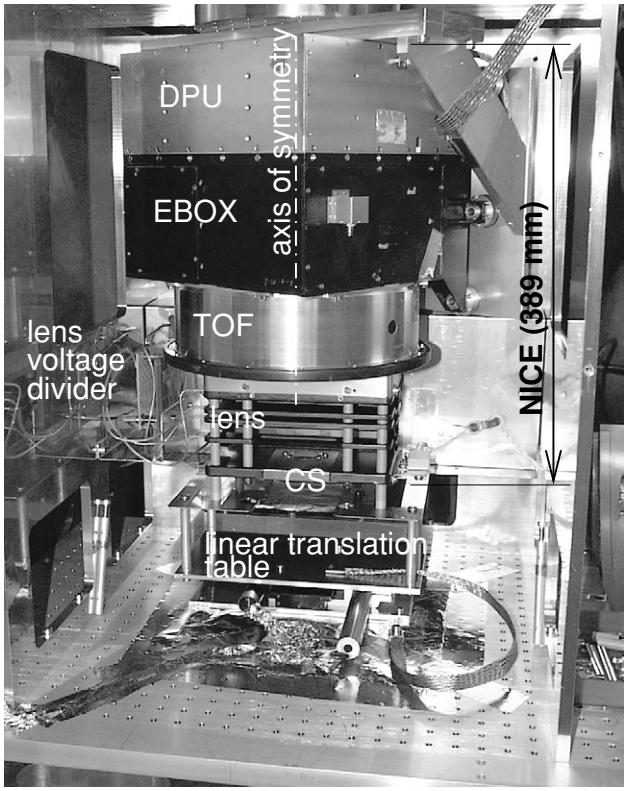

Figure 2. NICE prototype installed in the CASYMS [22] calibration facility at the University of Bern. Most electrostatic shielding and the ion beam neutralizing unit with the collimating entry aperture were removed for this picture. The small circular feature on the lowest plate in the lens right above the label 'CS' is the conversion surface. The time-of-flight mass spectrometer above the lens is an adapted flight spare unit of the composition and distribution function analyser (CODIF) as being flown on the Cluster satellites [21]. The time-of-flight section is labelled TOF, the electronics box containing the preamplifiers and the power supplies for the micro-channel plates EBOX, and the associated digital processing unit DPU.

CODIF; only one single angular pixel of the TOF section was illuminated. Furthermore, the charged particle deflection plates in front of the CS were integrated into the neutral beam source. The ion energy at the exit of the lens was high enough to achieve reasonable detection efficiencies for all measured species overcoming the inherent decrease in the detection efficiency of the TOF below 1 keV per nucleon due to the carbon foils used in the TOF to produce the start pulse. The extraction lens assembly including the CS was mounted on a linear translation table to allow for the scanning motion of the TOF entry aperture relative to the lens exit slit to achieve a coarse primary energy resolution. Figure 2 shows the prototype installed in the CASYMS calibration facility.

In a flight instrument the scanning will be performed by either varying the overall lens voltage or using a position resolving TOF system as is being used on IMAGE/LENA. In the prototype the conversion surface was maintained at −19 kV potential. The negative ions from the conversion surface are then accelerated towards the −5 kV potential at the entrance aperture of the TOF and finally hit the detectors, where the signal is picked up with reference to the ground potential. In a flight instrument the potential stack would be shifted such that the conversion surface is at ground potential

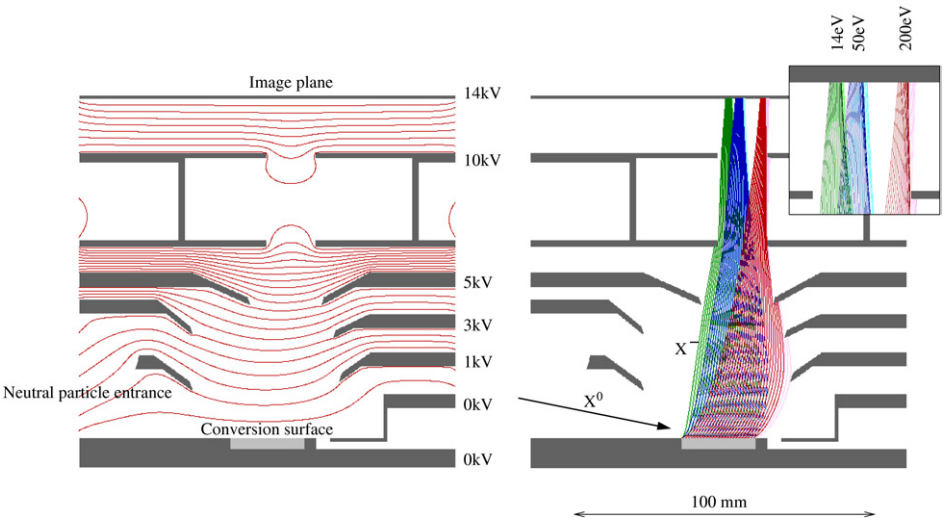

Figure 3. SIMION ion-optical simulation of the extraction lens. Equipotential lines with 500 V step size are shown in the left panel. Particle traces with different energies are shown in the right panel. Dark colours correspond to an angle of 65° and light colours to an angle of 82° to the surface normal at the conversion surface. Only a minor dependence of the position in the image plane on the angle of incidence at the conversion surface is visible (inset).

as shown in figure 3. The drawback of the configuration with the conversion surface at high negative voltage is increased background signal from sputtered ions caused by positive background ions accelerated towards the conversion surface. This was largely mitigated by thorough electrostatic shielding of the prototype. The instrument was mounted on a turntable to vary the incidence angle of the primary neutral atom beam relative to the conversion surface.

3. Neutral beam sources

Neutral particle sources from two independent facilities, University of Bern and University of Denver, were used for our investigations. In the Calibration System for Mass Spectrometers (CASYMS) facility [22] at the University of Bern a neutral atom beam was produced by reflection of a low energy positive ion beam from a single crystal tungsten surface. This technique for production of energetic neutral atoms is also used in surface science experiments [23]. Most ions are neutralized (>90%) and molecules mostly dissociate upon reflection allowing us to use positive molecules as primary particles as well. Molecular ions are produced very efficiently in the CASYMS ion source. The particles experience an energy loss of approximately 15% upon reflection [15, 16]. After the reflection the remaining charged particles are removed by an electrostatic deflection system. Apertures were used to limit the angular spread down to 3.6° × 27° FWHM. The energy distribution of the neutral beam was peaking at 85% of the primary ion energy with a width of approximately 10% of the primary energy [16]. The neutral flux is estimated by measuring the primary ion flux and by using the scattering and neutralization properties of the tungsten neutralization surface, which were calibrated before in the Imager for Low Energy Neutral Atoms (ILENA) facility at the University of Bern [16].

The test facility at the University of Denver supplied an intense pencil-like mono-energetic neutral beam [24]. This neutral atom beam is produced by photo-detaching electrons from negatively charged primary ions. An Ar-ion laser photo-detaches electrons from a fraction of the incident negative ions (<1%). After removal of the surviving ions, a neutral atom beam remains. The neutral flux is measured by modulating the laser intensity with a chopper wheel resulting in a modulation of the fraction of photo-detached particles. The modulation amplitude of the collected current of the remaining ions at the charged particle deflection plates is equivalent to the neutral particle flux. This source has the advantage of high neutral atom production rate at very low energies (∼20 eV) because at lower energies it takes longer for a particle to cross the laser interaction region. Therefore the probability for electron photo-detachment for an ion increases.

4. Results

The prototype instrument was extensively characterized. This included measuring the sensitivity of the instrument to varying angles of incidence of the primary beam, the energy resolution of the extraction lens, the overall detection efficiency of the instrument dependent on primary energy, and the separation of converted primary neutrals from sputtered particles from the conversion surface.

4.1. Extraction lens

Figures 4, 5 and 6 show ion-optical tests of the extraction lens. An ion beam with a cross section of 20 × 1 mm^2 was used to map out the ion-optical response of the extraction lens. For these measurements the conversion surface was replaced by a grid through which the ion beam entered. At the exit of the extraction lens an imaging detector was used. The traces in figures 5 and 6 show collapsed images along the energy dispersive axis of the lens exit. The set of measurements in figure 5 emulates the angular spread of the particles around the specular direction when scattered off the conversion surface. In this case the range of incident angles through the grid

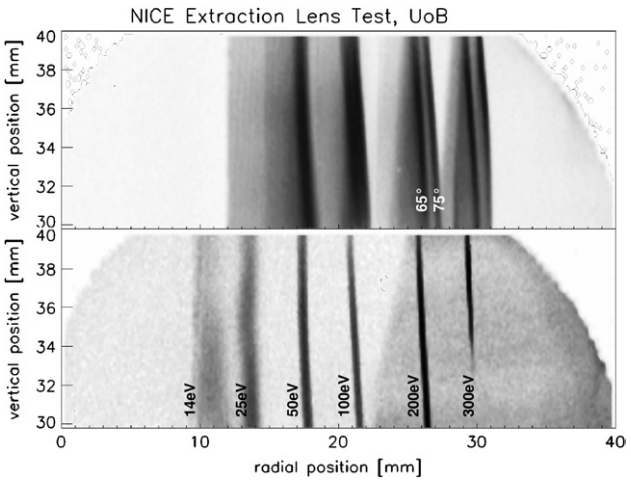

Figure 4. Energy resolving power of the extraction lens measured with an imaging detector placed at the exit of the lens. The response of the lens to beam energies from 14 eV to 300 eV at a constant angle of 75° to the conversion surface normal is shown in the lower panel. The upper panel shows the response to two different angles, 65° and 75°, for energies of 50 eV to 300 eV. As shown in figure 3, angular focusing improves towards lower energies. The arc-like structure in both panels is due to the field of view of the detector used. Note that the colour scales of the two panels are both logarithmic and also different to enhance the visibility of details.

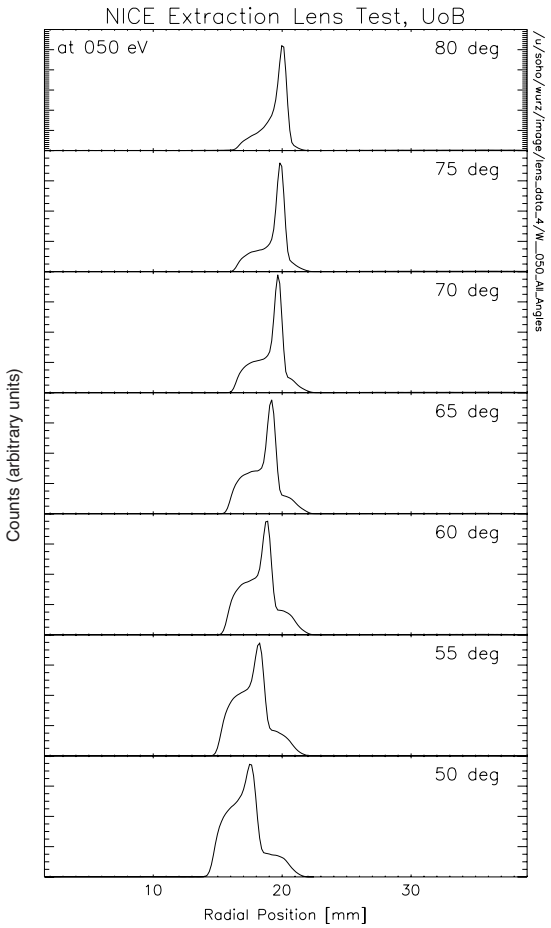

Figure 5. Result of ion-optical tests of the extraction lens. The seven panels show traces for a beam energy of 50 eV for a range of incident angles measured from the surface normal.

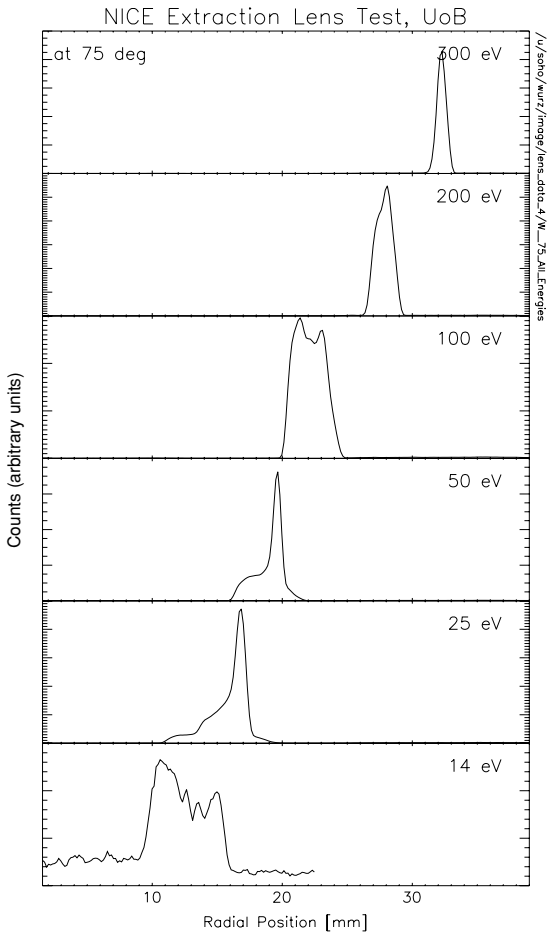

Figure 6. The six panels show traces for energies in the full range, the extraction lens is designed for an incident angle of 75° with respect to the surface normal.

represent a specular reflection angle of 65°, with ±15° of scattering about the specular direction. As one can see from the figure, ions leaving the conversion surface at these angles are all focused to a line. At energies of 200 eV and more, the angular focusing is degraded. However, the effect is still less than the energy dispersion.

Figure 6 shows energy dispersive properties of the extraction lens for 75° angle of incidence. For an actual instrument incident angles between 80° and 70° with respect to the surface normal are considered, with the NICE prototype using 82° as the nominal value. Clearly, the energy dispersive property of the extraction lens can be seen, which relates a radial position at the exit plane to an initial energy of the ion leaving the plane of the conversion surface. Shoulders at some of the peaks and the double peak structure in the 100 eV panel are introduced due to the finite mesh size of the grid. At 14 eV ion energy there was the additional problem of accurately setting the beam energy, which caused a broadening of the line.

4.2. Angular sensitivity

The scattering properties of a conversion surface depend strongly on the angle of incidence of the primary particles [16]. In the Denver facility, the angle between the incident

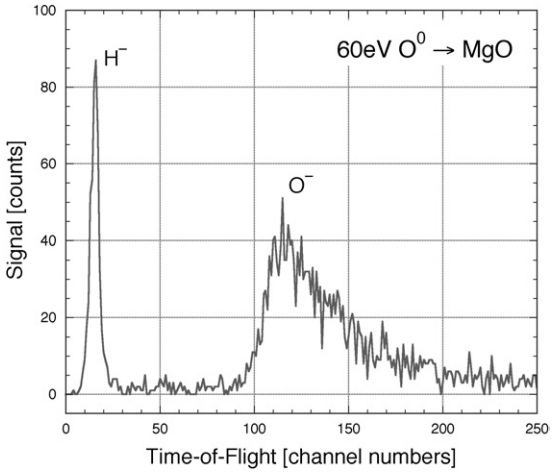

Figure 7. Sample TOF spectrum out of a scan over the exit of the extraction lens when using a 60 eV neutral oxygen primary beam and a MgO conversion surface. The time of flight increases with channel number.

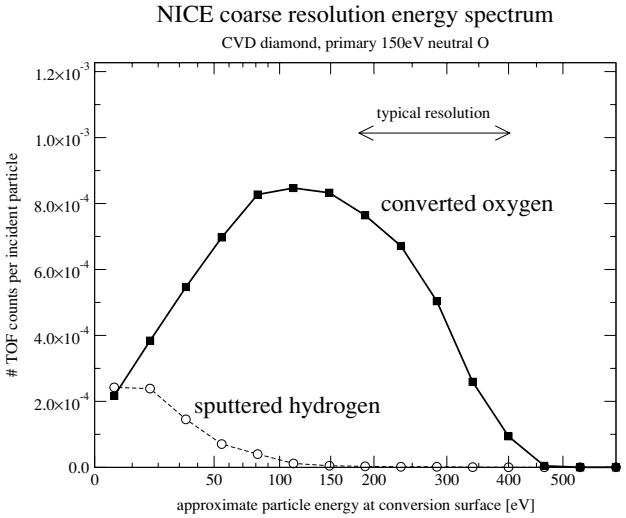

Figure 8. Scan over the exit of the extraction lens. Neutral oxygen was used as primary beam and negative charged particles were collected.

neutral beam and the surface normal was varied from 76° to 84°. However, because of the angular focusing of the extraction lens (figures 4 and 5), no significant dependence of the detection efficiency on the angle of incidence was observed. Variations were observed in the count rate due to the relatively small size of the conversion surface used (25 mm diameter) and small beam misalignments on the order of a fraction of a millimetre.

4.3. Energy resolution and sputtering

The energy resolution of the system was investigated by scanning the TOF entry aperture over the exit aperture of the extraction lens. For each position a TOF spectrum was taken. Figure 7 depicts a sample TOF spectrum obtained with a 60 eV neutral oxygen primary beam and a MgO conversion surface installed. The negative oxygen peak consists of the converted primary particles and a small fraction of sputtered particles (estimated to be <10% of the total oxygen counts). This upper limit results from measurements at higher energies (300 eV) where the extraction lens separates the sputtered and the converted particle fraction. The hydrogen peak is entirely due to sputtering of surface adsorbates by the primary particles. The sputtered fraction decreased considerably during the two days the surface was under test whereas the conversion efficiency for oxygen remained unchanged.

Figure 8 depicts an energy scan performed by varying the TOF entry slit position at the exit of the extraction lens when using a 150 eV primary oxygen beam and the CVD diamond conversion surface. After subtracting the background, fit functions were applied to the measured peaks in the TOF spectra to separate the observed species at each position at the exit of the lens. The approximate energy scale on the plot was obtained by using different primary energies and by observing the position of the maximum of the oxygen peak. The maximum represents 85% of the primary energy, as 15% is the approximate energy loss when reflecting a particle from the conversion surface [15, 16]. The peak is rather broad because the extraction lens has a limited energy focusing capability. That is further degraded by the finite entrance slit width of the TOF section (4 mm). Nevertheless, sputtered particles from the conversion surface can clearly be separated from converted incident neutrals. The energy distribution of the sputtered particles—mostly hydrogen—peaks at a few eV and consequently these particles appear on the low energy side of the spectrum.

4.4. Detection efficiency

The overall detection efficiency η_{total} of the instrument is a product of the efficiencies of the different subsystems and can be expressed as

$$\eta_{\text{total}} = \frac{F_{\text{measured}}}{F_{\text{incident}}} = \eta_i \eta_L \eta_F \eta_T$$

where F_{measured} represents the number of valid TOF counts per second, F_{incident} the number of incident neutral atoms per second that enter the instrument, η_i the fraction of particles that are negatively ionized upon reflection at the conversion surface, η_L the collection efficiency of the extraction lens, η_F the transmission of the C-foil in the TOF and η_T the detection efficiency of the TOF, which is species dependent. η_i shows a dependence on primary particle energy and species [15–17]. η_F and η_T depend on species and postacceleration voltage (14 kV in our case), the values used were taken from the CODIF calibration report [25]:

Species	η_F	η_T
Hydrogen	0.9	0.4
Oxygen	0.8	0.2

η_L depends only on the post-acceleration voltage as the initial neutral particle energy is much less than 14 keV per atom.

Using the known scattering and ionization properties of the conversion surfaces [15–17], the collection efficiency of the lens, η_L, was found to be in the range from 0.11 to 0.13 independent of the incident energy and species of the primary particles. The main energy dependence of the overall detection efficiency is thus caused by the energy dependence of the ionization efficiency.

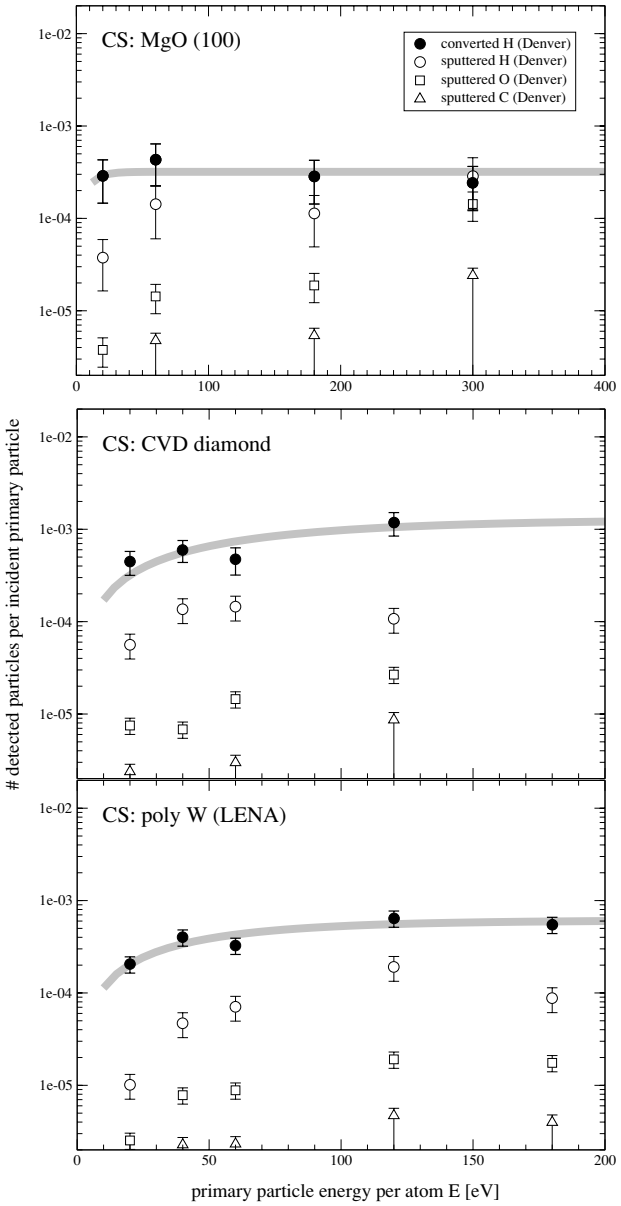

Figure 9. Detection efficiency for hydrogen obtained for different conversion surfaces (CS). Note the different energy axis scaling in the top panel.

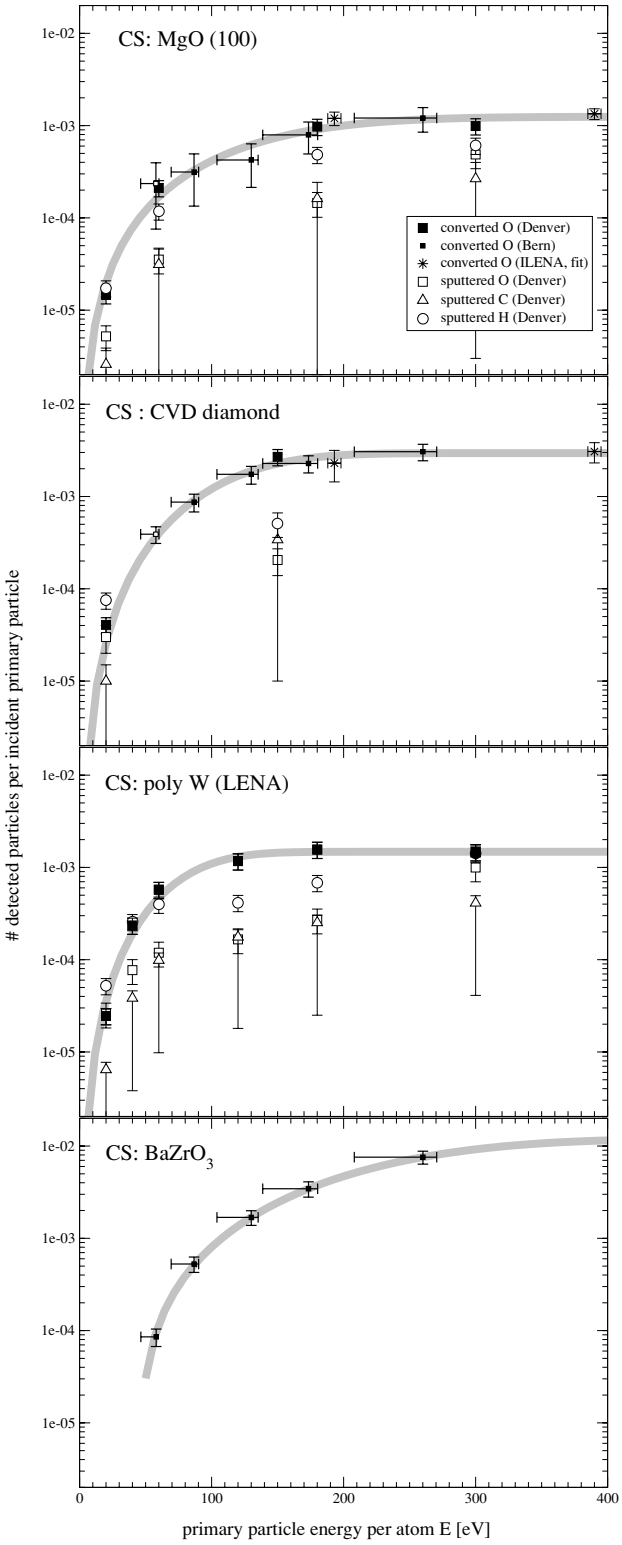

Figure 10. Detection efficiency for oxygen obtained for different conversion surfaces (CS). The data set labelled ILENA was taken from [16].

After subtracting the sputtered fraction, the overall detection efficiency is calculated by integrating over the energy distribution at the exit of the lens. Figures 9 and 10 depict the detection efficiency of the prototype for primary neutral oxygen and hydrogen for different conversion surfaces. The results obtained using the two different neutral beam sources, in Bern and Denver, agree very well (see figure 10, two topmost panels). The efficiencies for truly converted (ionized) atoms are presented with the probabilities for sputtering by primary atoms and background ions accelerated onto the conversion surface resulting in a detected ion. All combinations of primary atoms and conversion surfaces show an energy dependence with increasing efficiency at higher particle energy. The obtained detection efficiency data were fitted by simple exponential functions that are given as grey lines in figures 9 and 10. Figure 11 depicts a comparison of the instrument performance depending on primary energy, type of conversion surface, and primary species. In this summary plot only the empirical fits, shown as grey lines in figures 9 and 10, are given. For primary oxygen a strong energy dependence over several orders of magnitudes was observed

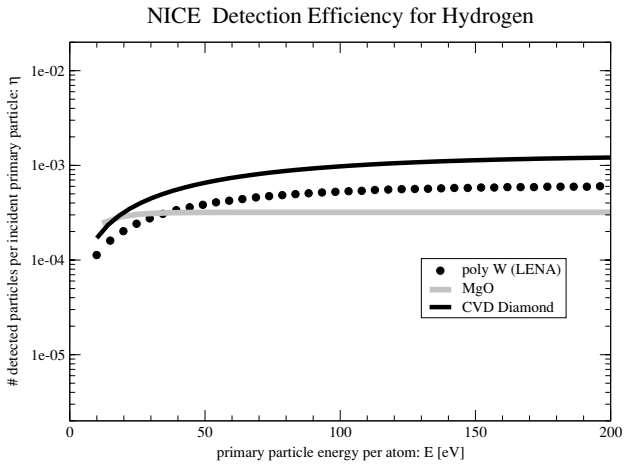

(*a*)

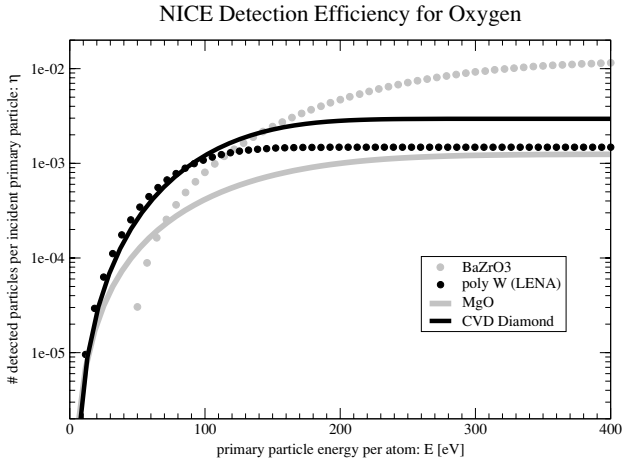

(*b*)

Figure 11. Summary of empirical detection efficiencies for different conversion surfaces.

at low energies, whereas for primary hydrogen the detection efficiency curves are almost flat in the investigated energy range.

4.5. Extracting positive ions

We have also considered using the fraction of positively ionized particles instead of the negative ions, which are also formed upon reflection from the conversion surface. When using positive ions contamination of the measurement by secondary and photoelectrons is not a problem, and their efficient suppression at the conversion surface will not be necessary. The detection efficiency obtained using the positive hydrogen fraction is shown in figure 12. For energies higher than 150 eV the detection efficiency is higher than the detection efficiency obtained using the negative ion fraction (figure 9, second panel from top) but at lower energies the detection efficiency drops very fast. As interstellar hydrogen arrives with at most 30 eV in the spacecraft reference frame, the negative ion fraction is preferable because of the higher detection efficiency. Oxygen is not detectable when using the positive ion fraction, because the positive oxygen ion fraction after reflection off the conversion surface is very small (<1%), even at energies up to 2 keV [16, 26]. Using the positive

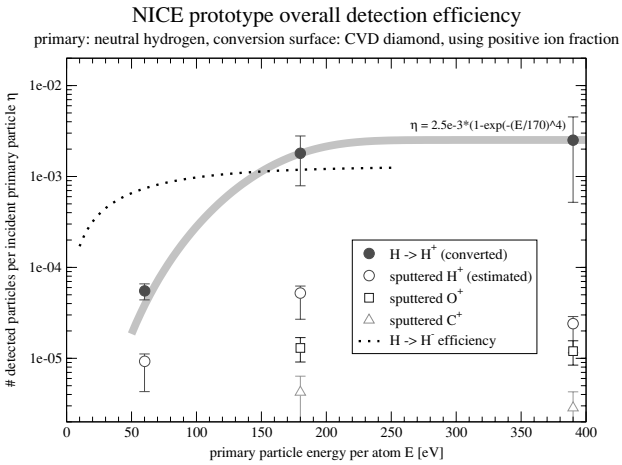

Figure 12. Detection efficiency for primary hydrogen and the CVD diamond conversion surface when using the positive ion fraction. The detection efficiency obtained when using the negative charge state fraction is shown for comparison (dotted line, from figure 9, middle panel).

ion fraction does not seem to be an attractive option for an interstellar neutral gas instrument for the energy range and the species of interest.

5. Discussion

5.1. Extraction lens

The energy resolving capabilities of the extraction lens were found to be according to ion-optical simulations. Given the energy spread a particle experiences at the conversion surface, the resolving power of the extraction lens is close to the optimum value. A flight version of the lens would benefit from anti-reflective surface coating of the lens electrodes to minimize signals originating from particles reflected or sputtered at structure parts. While not a problem in the prototype the measured background could be reduced significantly, thus enlarging the dynamic range.

5.2. Angular sensitivity

No dependence of the detection efficiency on the angle of incidence in the range of 76° to 84° was found. This is consistent with earlier findings [16] that showed no dependence of the ionization efficiency of a conversion surface on the angle of incidence for angles between 80° and 85°. Although the width of the angular scattering distribution increases at steeper angles and also at higher particle energies, the extraction lens can focus these angular distributions sufficiently well.

5.3. Energy resolution and sputtering

The energy resolving capability of the extraction lens allows for the separation of sputtered particles from converted incident neutrals. The energy distribution of the sputtered particles peaks at a few eV, thus all sputtered particles appear at the low energy side of the energy spectrum. Hydrogen is the predominant species sputtered from the conversion surface (figure 7). The main sources for sputtering particles will be

primary helium, carbon and oxygen neutral atoms as they are the most abundant elements to which the instrument is sensitive after hydrogen. Sputtering due to primary hydrogen is unlikely because of the low energy of the neutral hydrogen atoms (70 km $s^{-1} \approx 25$ eV) and the low mass. Assuming a CVD diamond conversion surface and using elemental abundances of the neutral interstellar inflow from [27], hydrogen sputtered by incident oxygen atoms at a velocity of 70 km s^{-1} would contribute about 1% to the total hydrogen counts; about 4% of the hydrogen counts will be due to sputtering by helium. Effects that modify the elemental abundances, i.e., at the heliospheric interface, are neglected in this estimation.

In the LISM, oxygen has an abundance of approximately 5×10^{-4} relative to hydrogen and the sputtering efficiency for hydrogen atoms is about 10^{-3} (from figure 10, middle panel). The fraction of sputtered hydrogen due to neutral oxygen is therefore of the order of 5×10^{-7} per incident neutral hydrogen atom, far less than the detection efficiency for an incident 70 km s^{-1} hydrogen atom at 5×10^{-4}. Thus, hydrogen sputtered by incident oxygen should amount to about 1×10^{-3} of the hydrogen counts.

Hydrogen sputtered by incident helium gives stronger constraints: when estimating [28] the sputtering efficiency for helium using the hydrogen and oxygen data, a sputter yield of 1×10^{-4} is obtained for helium atoms at 70 km s^{-1}. Combined with a helium abundance in the LISM of approximately 0.1 relative to hydrogen, 2×10^{-5} hydrogen counts due to sputtering by helium are expected per incident neutral hydrogen. This yields a 4% contribution to the hydrogen atom signal.

In our experiment, the conversion surface was transferred from air into vacuum and measurements were started approximately one day later when the pressure in the vacuum chamber was below 10^{-6} mbar. In the first few hours of measurement a systematic decrease in the sputter rate was observed, indicating outgassing and conditioning of the surface with time. The observed sputter rates are thus considered upper limits. On a mission heading out to the heliopause the instrument would have several years to outgas in a much better vacuum. The NICE instrument could also be combined with a GAS type instrument sensitive to helium to better estimate the sputter rate and also to extend the elemental range to helium.

5.4. Conversion surfaces

Of the four different investigated conversion surfaces, $BaZrO_3$, MgO, CVD diamond and tungsten, the CVD diamond surface exceeds all others in performance except for oxygen at energies above 150 eV per atom where $BaZrO_3$ shows better performance (figure 11). Unfortunately, the ionization yield for neutral oxygen of the $BaZrO_3$ surface drops very fast below 150 eV per atom. CVD diamond does not show this limitation. The hydrogen terminated CVD diamond surface is furthermore mechanically and chemically very stable and can be polished down to a few nm_{rms} for optimized scattering properties. Although the sample used was a custom made surface, a similar commercially available material, tetrahedral amorphous carbon (ta-C) films, a subset of diamond-like carbon (DLC) films, was recently shown to have approximately equal performance [29]. The bulk materials tungsten and MgO are less favourable, the ionization efficiency of tungsten at low energies depends strongly on surface adsorbates and the insulating properties of MgO cause charging problems due to photoelectrons when illuminated by UV radiation.

5.5. Instrument detection efficiency

Assuming a interstellar neutral density for hydrogen of 0.1 cm^{-3} and an apparent inflow velocity of 70 km s^{-1} (as seen from a spacecraft), locking into the apparent inflow direction, and integrating over the whole angular distribution approximately 75 counts/s for hydrogen and 0.35 counts/s for oxygen can be expected using the current prototype with an active area of 0.35 cm^2.

Without significant changes in the design, the count rate can be increased by a factor of 4 by increasing the open area of the instrument. This is achieved by three measures: the size of the CS is increased from 25 mm to 40 mm in the radial direction away from the axis of symmetry, the size of the pinhole in the azimuthal plane is increased until its matches the azimuthal resolution of the TOF of 22.5°, and the average angle of incidence to the CS is changed from 82° to 78°. This will result in an open area of 1.4 cm^2. All three modifications require no change of the ion-optics of the extraction lens. The CS size presently used for the NICE prototype was chosen for cost reasons. Simulations using SIMION show that the present extraction lens is capable of collecting particles from a larger CS area without significant losses.

Another factor of 2 can be obtained by optimizing the extraction lens and the interface between the extraction lens and the TOF. A smaller part of this factor will be obtained by optimizing the field shaping electrodes above the CS using numerical methods. The larger part will be gained by removing the defocusing properties of the TOF entry aperture plate.

A factor of 1.5 is feasible by optimizing the TOF unit itself. For the NICE prototype, the TOF unit was operated with signal outputs referenced to ground potential and with lower internal acceleration voltages in order to reduce the maximum voltage present in the setup to 19 kV. A TOF unit specifically designed for this application would not be subject to these limitations and therefore have a larger sensitivity.

By combining all these improvements count rates of 900 counts/s for hydrogen and 4.2 counts/s for oxygen would be obtained.

Further optimizations are possible by switching from a 1D-pinhole camera type sensor to a single pixel telescope as used in the GAS instrument. Although major modifications to the ion-optics would be necessary, this would increase the collection efficiency of the lens to almost 100%, as also particles scattered in the azimuthal direction could be focused onto the detector. The detection efficiency would increase by a factor of 3 to 4 compared to the optimized 1D-pinhole camera sensor. Consequently, count rates up to 3600 counts/s for hydrogen and 17 counts/s for oxygen are possible. A single pixel telescope would also allow us to increase the open area as proposed for the Neutral Atom Telescope (NAT) sensor

of the Interstellar Neutral Atom Detector (INAD) [30], where 38 cm^2 open area is used compared to 1.4 cm^2 in the optimized 1D-pinhole camera sensor. The single pixel telescope arrangement is offset by the need for a scanning platform to measure the full sky angular distribution as used by the GAS instrument or proposed for the INAD instrument or the need to change the pointing of the spacecraft on a regular basis as is done on the IBEX mission [11].

6. Conclusion

We have successfully tested a prototype for an instrument for the direct measurement of the interstellar neutral gas. The results from two independent facilities agree very well. The detection efficiency of the present instrument is high enough to get reasonable counting statistics within hours. Sputtered and converted primary neutrals can be separated by their characteristic energies when leaving the conversion surface. The detection efficiency of the prototype can be increased up to a factor of 3 for the design used for the prototype and a factor up to 12 when changing to a single pixel telescope. NICE is planed to be part of the scientific payload of a new interstellar medium exploration spacecraft to be proposed in the MIDEX spacecraft class of NASA's Explorer Program, currently scheduled for the years 2011–2012.

Acknowledgments

The authors thank Matthias Boehm, Ken Crocker, and Mark Granoff for their support when performing the experiments and Adrian Etter for the operation of the CASYMS chamber. This work is supported by the Swiss National Science Foundation and by NASA Grant NAG5-8733.

References

[1] Fahr H-J 2004 Global structure of the heliosphere and interaction with the local interstellar medium: three decades of growing knowledge *Adv. Space Res.* **34** 3–13

[2] Thomas G E 1978 The interstellar wind and its influence on the interplanetary environment *Ann. Rev. Earth Planet* **6** 173–204

[3] Witte M, Banaszkiewicz M, Rosenbauer H and McMullin D 2004 Kinetic parameters of interstellar neutral helium: updated results from the ULYSSES/GAS-instrument *Adv. Space Res.* **34** 61–5

[4] Zank G P and Pauls H L 1996 Modelling the heliosphere *Space Sci. Rev.* **78** 95–106

[5] Gruntman M, Roelof E C, Mitchell D G, Fahr H J, Funsten H O and McComas D J 2001 Energetic neutral atom imaging of the heliospheric boundary region *J. Geophys. Res.* **106** 15767–81

[6] Witte M, Rosenbauer H, Keppler E, Fahr H, Hemmerich P, Lauche H, Loidl A and Zwick R 1992 The interstellar neutral-gas experiment on ULYSSES *Astron. Astrophys.* **92** 333–48

[7] Ghielmetti A G, Shelley E G, Fuselier S, Wurz P, Bochsler P, Herrero F, Smith M F and Stephen T 1994 Mass spectrograph for imaging low energy neutral atoms *Opt. Eng.* **33** 362–9

[8] Wurz P, Aellig M R, Bochsler P, Ghielmetti A G, Shelley E G, Fuselier S A, Herrero F, Smith M F and Stephen T S 1995 Neutral atom imaging mass spectrograph *Opt. Eng.* **34** 2365–76

[9] Moore T E *et al* 2000 The low-energy neutral atom imager for IMAGE *Space Sci. Rev.* **91** 155–95

[10] Gloeckler G *et al* 1998 Interstellar Pathfinder—a mission to the inner edge of the interstellar medium, A proposal to NASA in response to AO 98-OSS-03 for a medium-class explorer

[11] McComas D J *et al* 2004 The Interstellar Boundary Explorer (IBEX) *Physics of the Outer Heliosphere: 3rd Int. IGPP Conf. (AIP Conf. Proc.* vol 719*)* ed V Florinski, N V Pogorelov and G P Zank pp 162–81

[12] McNutt R L *et al* 2002 A realistic interstellar explorer *Solar Wind Ten: Proc. 10th Int. Solar Wind Conf. (AIP Conf. Proc.* vol 679*)* ed M Velli, R Bruno and F Malera pp 830–3

[13] Liewer P, Mewaldt R, Ayon A and Wallace R 2000 NASA's interstellar probe mission *Technical Report* NASA Jet Propulsion Laboratory, Space Technology and Application International Forum STAIF

[14] Wurz P 2000 Detection of energetic neutral particles *The Outer Heliosphere: Beyond the Planets* (Katlenburg-Lindau: Copernicus Gesellschaft e.V.)

[15] Jans S, Wurz P, Schletti R, Brüning K, Sekar K, Heiland W, Quinn J and Leuchter R E 2001 Negative ion production by surface ionization at barium zirconate surface *Nucl. Instrum. Methods* B **173** 503–15

[16] Wieser M, Wurz P, Brüning K and Heiland W 2002 Scattering of atoms and molecules off a magnesium oxide surface *Nucl. Instrum. Methods* B **192** 370–80

[17] Wurz P, Schletti R and Aellig M R 1997 Hydrogen and oxygen ion production by surface ionization using diamond surfaces *Surf. Sci.* **373** 56–66

[18] May P W 2000 Diamond thin films: a 21st-century material *Phil. Trans. R. Soc.* A **358** 473–95

[19] Yanochko R, Brock W, Krzanowski J, Quinn J and Leuchtner R E (ed) 1996 Pulsed laser deposition of barium zirconate thin films for neutral particle imaging applications *Mat. Res. Soc. Symp. Proc. (Boston, MA, USA, 1–6 Dec.)*

[20] Inc. Scientific Instrument Services, *SIMION 3D Version 7.0 Ion Optics Program*, 1996–2005 1027 Old York Road, Ringoes, NJ 08551, USA

[21] Rème H *et al* 1993 The Cluster Ion Spectrometry Experiment *ESA SP-1159*

[22] Ghielmetti A G, Balsiger H, Bänninger R, Eberhardt P, Geiss J and Young D T 1983 Calibration system for satellite and rocket-borne ion mass spectrometers in the energy range from 5 eV/q to 100 keV/q *Rev. Sci. Instrum.* **54** 425–36

[23] Losch A and Niehus H 1999 Structure analysis of the kBr(100) surface—an investigation with a new method for surface analysis on insulators *Surf. Sci* **420** 148–56

[24] Stephen T M, van Zyl B and Amme R C 1996 Generation of a fast atomic-oxygen beam from O^- ions by resonant cavity radiation *Rev. Sci. Instrum.* **67** 1478–82

[25] Kistler L M 2000 Cluster CODIF calibration report *Technical Report* University of New Hampshire, NH, USA

[26] Verbeek H, Eckstein W and Bhattacharya R S 1980 Negative hydrogen ion formation by backscattering from solid surfaces *Surf. Sci.* **95** 380–90

[27] Geiss J and Witte M 1996 Properties of the interstellar gas inside the heliosphere *Space Sci. Rev.* **78** 229–38

[28] Taglauer E 1990 Surface cleaning using sputtering *Appl. Phys.* A **51** 238–51

[29] Scheer J A, Wieser M, Wurz P, Bochsler P, Hertzberg E, Fuselier S A, Koeck F A, Nemanich R J and Schleberger M 2005 High negative ion yield from light molecule scattering *Nucl. Instrum. Methods* B **230** 330–9

[30] Levi S, Moebius E, Haggerty D, Witte M and Wurz P 2002 An Interstellar Neutral Atom Detector (INAD) *Solar Wind Ten: Proc. 10th Int. Solar Wind Conf. (AIP Conf. Proc.* vol 679*)* ed M Velli, R Bruno and F Malera pp 850–3